npj | flexible electronics

Article

Published in partnership with Nanjing Tech University

https://doi.org/10.1038/s41528-025-00472-x

A fully-integrated flexible in-sensor computing circuit based on gel-gated organic electrochemical transistors

Xinyu Tian, Jing Bai, Dingyao Liu, Guangxi Lu & Shiming Zhang ✉

Organic electrochemical transistors (OECTs) are promising technologies for biosensing and brain-inspired computing due to their low-power signal amplification and neuron-like behavior. However, their manufacturing remains complex, especially when fabricated into flexible forms. To address the growing demand for flexible OECTs in wearable bioelectronics, in this work, we propose: **i)** a rapid and low-cost fabrication approach using flexible PCB (fPCB) technology and customized inkjet printing; **ii)** a non-aqueous gel-gated approach to improve the electrochemical stability of flexible OECTs associated with fPCBs; and **iii)** the above two approaches help accomplish the following concept: low-cost, integrated, and in-sensing computing system can be more readily realized with flexible OECT devices. This platform has been validated for scalability, stability, and performance in real-world applications, paving the way for developing low-cost, flexible, multifunctional OECT systems.

Organic electrochemical transistors (OECTs) are being pursued as promising technologies for emerging biosensing and bioelectronics applications due to their ability to amplify weak biosignals at extremely low power[1–5]. This unique capability makes them highly attractive for in-sensor computing applications where signal processing and amplification are integrated[6]. The typical OECT device structure is composed of gate, source, and drain electrodes, an organic semiconductor channel, and an electrolyte[7–9]. The channel is patterned between the source and drain electrodes. The electrolyte is in direct contact with the conducting polymer channel, such as poly(3,4-ethylenedioxythiophene): poly(styrene-sulfonate) (PEDOT:PSS). When a positive (negative) gate voltage (V_{gs}) is applied, the cations (anions) in the electrolyte are electrostatically repulsed into the channel, and an electrochemical dedoping (doping) process subsequently occurs. This process manipulates the conductivity of the channel[10–12].

In recent years, flexible OECTs have been pursued by the community to facilitate their use for emerging bioelectronic applications, such as medical wearables and implantables[5,13–19]. Besides, because the ion-diffusion is a dynamic and non-linear process, OECT is thus a non-linear device, making them potential hardware candidates to simulate the non-linear computing behavior of neurons and enabling in-sensor computing applications[20–25]. Despite the rapid growth, the manufacturing of flexible OECTs is time-consuming and suffers a low device yield, partially due to the complicated electrode patterning process on plastic and the poor adhesion between layers on flexible substrates. Besides, additional steps are needed to pattern the insulating layers to protect the electrodes[13,26,27]. Therefore, great efforts have been dedicated to simplify the fabrication process of flexible OECTs[28–30]. Meantime, it is expected that fast turnaround time, low fabrication cost, and high device yield can be achieved at the same time.

Flexible printed circuit board (fPCB) manufacturing technologies have become successful in the past decades and are now widely used in the industry[31]. It allows standardizable manufacturing of large-scale flexible electronic circuits at a low cost and fast turnaround time. However, the OECT community has not taken much advantage of this mature manufacturing technology. A main challenge is that the fPCB process mostly uses copper as the prior material for electrode fabrication, which is not favored in an electrochemical (EC) system because of the poor electrochemical stability of copper in air and water. Besides, the fPCB process does not involve the patterning of the conducting polymer channel—a critical component for OECTs[32]. Therefore, a fast, reliable, and scalable channel patterning method is yet to be introduced to marry the fPCB process.

Here, we report a printing-based and scalable manufacturing method for rapidly prototyping flexible OECTs devices and circuits, specifically tailored for in-sensor computing applications. The electrodes, interconnects, and insulators were first fabricated with the commercial fPCB process, followed by patterning the channel and electrolyte with an inkjet printing process. Gold-protecting layers and gel-based electrolytes are used to mitigate the redox reaction of the copper. The feature size (channel length) of the devices is about 100 μm. The device yield, device-to-device variation, and stability were verified, comparable to the state-of-the-art methods, but the process is more efficient in time and cost. The fabrication of electrode arrays with channel length down to 100 μm can be completed within 24 h at a cost of approximately USD 10 per square meter, which

Department of Electrical and Electronic Engineering, The University of Hong Kong, Pokfulam, Hong Kong.
✉e-mail: beszhang@hku.hk

avoids the need for expensive and complex cleanroom facilities and environments, thereby lowering the entry barriers for OECT design and prototyping. This strategy enables rapid prototyping of neuromorphic computing units, low-cost biosensors, and fully integrated in-sensor computing systems for wearable bioelectronics. As an example, we demonstrate the use of this strategy for the rapid prototyping of flexible and all-solid-state OECTs for neuromorphic in-sensor computing applications.

Results and discussion

Design of the fully integrated flexible in-sensor computing circuit

Figure 1 illustrates the design of an in-sensor computing system based on fPCB-fabricated, non-aqueous gel-gated OECTs. The fully integrated system combines a wireless readout circuit with an OECT array for simultaneous biosensing and biocomputing (Fig. 1b–d). As shown in Fig. 1e, built on an fPCB, the system incorporates power management modules, analog front-end modules, and a built-in Bluetooth-Low-Energy (BLE) microcontroller for real-time signal acquisition and transmission.

Fabrication of OECT arrays on fPCB

Figure 1c illustrates the resultant electrode arrays of 36 OECT units and the schematic of the single OECT device. A total of 108 interconnects were integrated within an area of 5 cm * 8 cm on the same layer. The feature size is about 100 μm, with channel width/length down to 100/100 μm. The fabrication of the electrodes of flexible OECTs starts with the photolithographic patterning of copper electrodes on the polyimide (PI) substrate, followed by the electroplating of a thin layer of gold (20 nm) to protect the copper (Fig. S1). The electrodes were further encapsulated by a second layer of PI (detailed in the experimental part).

Despite being protected with the gold layer (20 nm), Cu electrodes remain suffer from a redox instability with the electrolyte. This indicates the aqueous electrolyte can leak to the Cu layers to react. The reaction became noticeable at increased positive scanning voltages (> 0 V), limiting the use of fPCB-fabricated electrodes in water and aqueous hydrogel[33]. Nevertheless, we found the use of gel-based electrolytes (Fig. 2a) can efficiently mitigate the redox reaction of the Cu electrodes. As shown in Fig. 2b and Fig. S2, a negligible redox current was observed when the voltage was scanned between -1 V and +1 V, a typical voltage-operation window of OECTs. The results indicate the gel electrolytes can efficiently curb the diffusion of ions to the underlying Cu electrodes, thus maintaining the high stability of the electrodes under cyclic voltammetry (CV) scanning.

The high stability of the fPCB-fabricated flexible electrode arrays in gel-electrolytes permits their use in developing all-solid-state devices and circuits. A typical application is to develop neuromorphic transistors to mimic the synaptic behaviors of neuron circuits[25]. For such applications, gel electrolytes are widely used and patterned between the gate and channel of OECTs to serve as ion reservoirs to regulate the device behaviors[34,35].

The all-solid-state OECTs were fabricated by first fabricating the electrodes with the fPCB process, followed by the patterning of PEDOT:PSS channel and the gel electrolyte with a customizable inkjet printer (Fig. 2c), detailed in the experimental part). Crosslinkers were added to both the conducting polymer channel and the gel-electrolyte to improve their adhesion to the flexible substrates to prevent delamination over time and under bending conditions[26]. Because the feature size of the electrolyte is around 100 μm, alignment can be quickly completed between different functional layers.

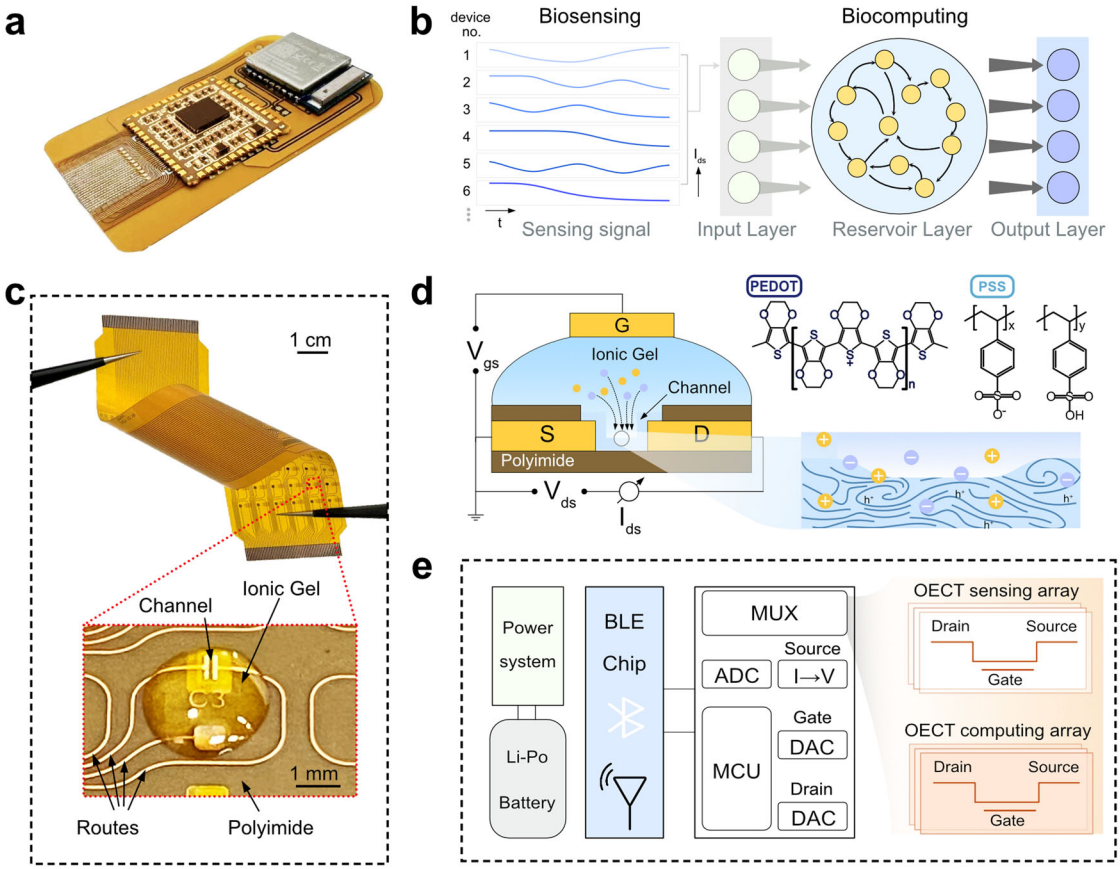

Fig. 1 | The design, architecture, and working principles of the fully integrated flexible in-sensor computing circuit based on non-aqueous gel-gated OECTs. **a** Real image of the fPCB-fabricated fully integrated flexible in-sensor computing system. **b** The mechanism of the OECT-based biosensing and biocomputing. **c** Real images of the fPCB- fabricated electrodes. **d** The schematic of an OECT device. **e** Logic diagram of fully integrated flexible in-sensor computing circuits.

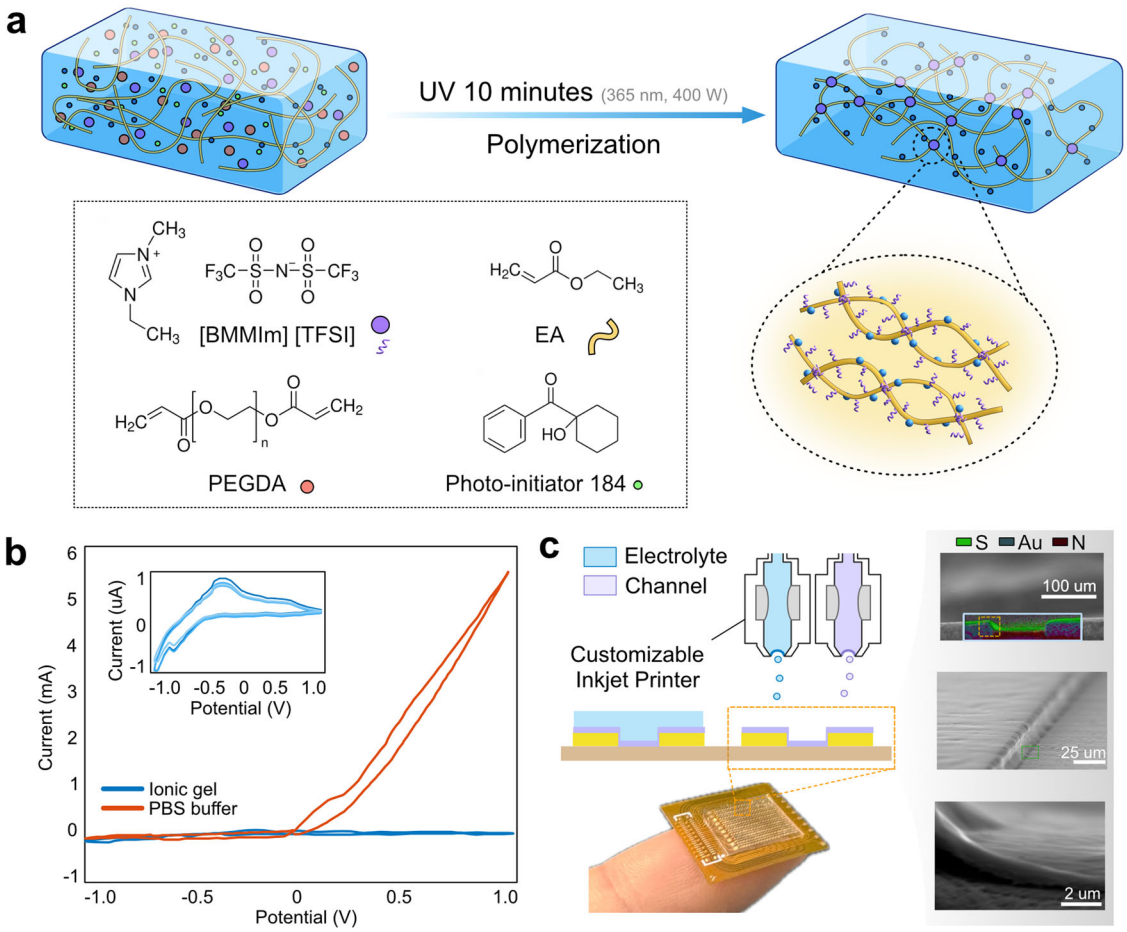

Fig. 2 | Material design of OECTs fabricated with fPCB technology and ink-jet printing. a Schematic and chemical structure of relevant chemicals to synthesize non-aqueous poly(ethyl acrylate) (PEA) ionic gel. **b** The comparison of CV curves of fPCB-fabricated electrodes (Au (200 nm)/Cu (30 μm)) with ionic gel and PBS as electrolytes, respectively. Inset: Zoom-in view of the CV response for the ionic gel. Three consecutive scans were performed to assess repeatability; the color intensity from dark to light blue represents the first to third scan, respectively. **c** Schematics of the customized inkjet printing platform for patterning of the channel and electrolyte. The scanning electron microscope (SEM) image shows the side-view of the interfaces between PEDOT:PSS channel and the electrodes.

OECTs characterizations

The overall performance of the resultant flexible all-solid-state OECTs is summarized in Fig. 3. Four types of typical curves were measured: output, transfer, transient, and cyclic stability. PEA was used as a solid-state electrolyte to prevent the reaction with copper electrodes. Gold-modified copper (area of 0.8 m^2, thickness, 35 μm) was used as gate electrodes. The devices showed typical transistor characteristics, working in depletion mode (Fig. 3a, b). A high on/off ratio of ~1000 was extracted from the transfer curves (V_{gs} from -0.2 V to 0.8 V, source-drain voltage (V_{ds}) from −0.1 to −0.6 V). Mobility of 1.1 $cm^2 V^{-1} s^{-1}$ is calculated according to the Bernards-Malliaras model[10] (Fig. S3), indicating the high quality of the fPCB-printed electrodes and the inkjet-printed channels. The transfer curves showed minor hysteresis (Fig. S4) and good repeatability under cyclic scanning of V_{gs} between −0.1 and 0.8 V, which is within the safe electrochemical window for cooper (Fig. 3c). Besides, the transient response remains unchanged after 60 cycles of gate pulses, demonstrating the high stability of the devices thanks to the use of hydrogel electrolyte to prevent the oxidation of copper and the excellent adhesion between function layers because of the use of crosslinkers (Fig. 3d). The transient response also indicated a relatively fast dedoping/dedoping process of the channel due to the small geometrical size of the devices.

Homogeneity and flexibility of the fPCB-fabricated OECT arrays

To gain insight into the homogeneity and flexibility of our printed PEDOT:PSS films and the assembled solid-state OECTs on fPCB, we measured the channel current (I_{ds}) and transconductance (g_m) of an array consisting of 200 devices (Fig. 4a). The statical results show that the device yield is close to 100%, without notable failure operation, indicating good device homogeneity was achieved, benchmarkable to those patterned with state-of-the-art perylene or orthogonal photoresists[36]. To evaluate the flexibility of the devices, bending tests were performed by laminating the devices on 3D-printed testbeds with gradually changed bending curvatures (Fig. 4b). The transfer curves of the devices showed negligible change upon increasing bending curvature, the same for the extracted g_m values, indicating the excellent conformability of the devices thanks to the thin thickness of the fPCB (thickness of 200 μm) and the improved softness of the PEDOT:PSS because the addition of stretchability enhancers (Fig. 4c, d)[37].

Tactile sensing evaluation of fPCB-fabricated flexible OECTs

It can be easily imagined that the proposed fPCB-based fast, low-cost, and scalable fabrication methods for flexible OECTs have wide applications (Fig. S5)[38]. To demonstrate, we first evaluated the biosensing capabilities of these flexible OECT arrays. Here, we propose a rapid customizing OECT-based tactile sensor by integrating a micropyramid-structured ionic gel gated electrode of the fPCB-fabricated flexible OECTs, making it suitable for future personalized precision medicine and human–machine interaction (Fig. 5). The sensing mechanism of the fPCB-based OECT tactile sensor is illustrated in Fig. 5a and detailed in our previously reported work[39]. As shown in Fig. 5b, the fPCB-based OECT biosensor demonstrated highly sensitive responses to a wide range of applied pressures, ranging from 0.1 to

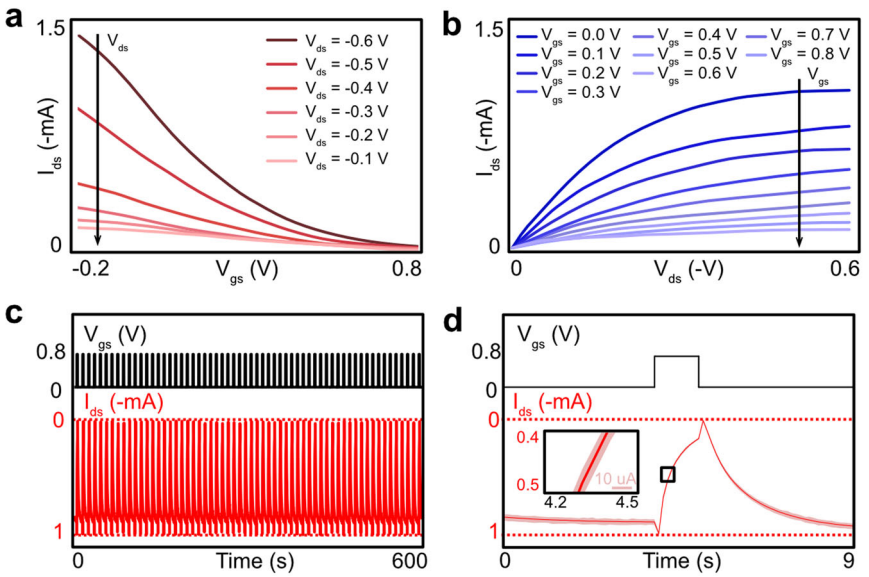

Fig. 3 | Electrical characterizations of OECTs fabricated with fPCB technology and ink-jet printing. a The transfer curves (V_{gs} scanned from −0.2 to 0.8 V) at different V_{ds} values (from -0.1 V to 0.6 V). **b** Output curves (V_{gs} scanned from 0 V to 0.8 V, V_{ds} scanned from 0 V to -0.6 V). **c** Transient curves: a group of 60 pulses with 1.25 s width and 800 mV amplitude were applied at the gate electrode. **d** The red solid line shows the average I_{ds} response of the 60 pulses in c) and the red shadow shows the current variation range during the transient characterization (< 10%), indicating the robustness of the device during cyclic measurements.

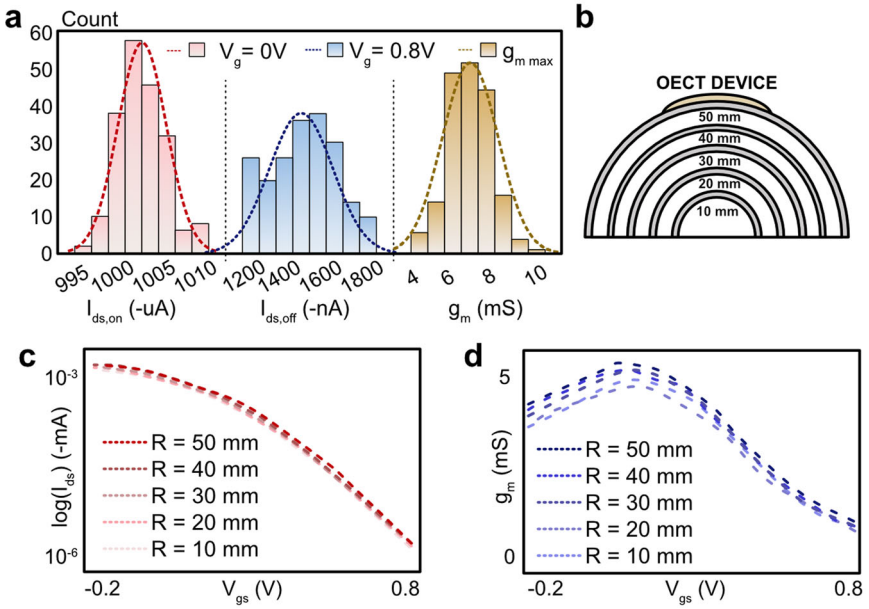

Fig. 4 | Homogeneity and flexibility characterizations of the flexible OECTs. a Comparison of channel currents at V_{gs} = 0 V, V_{gs} = 0.8 V and maximum g_m of 200 devices fabricated with fPCB technology. **b** Experimental setup of the flexibility test of OECTs. **c**, **d** Transfer and g_m curves under different bending radius (from 10 to 50 mm).

10 Pa. Figure 5c shows the hand-written experiment characters from "0" to "9" tested using the fPCB-based OECT tactile sensor array. Following binary processing and reshaping, the outcomes of the handwriting test with the tactile sensing array serve as the input dataset for the subsequent in-sensor computing process. The promising result from fPCB-based OECT tensile biosensors highlights its potential for real-time, reliable biosignals monitoring in precision wearable healthcare and human-machine interaction applications.

Neuromorphic function evaluation of fPCB-fabricated flexible OECTs

The high stability of the fPCB-fabricated flexible electrode arrays in gel electrolytes permits their use in all-solid-state devices. Another typical application of the device is to develop neuromorphic circuits to mimic the synaptic behaviors[25,40,41]. As shown in Fig. 5d, e, we further demonstrate the potential applications of those flexible OECT arrays with a specific neuromorphic computing framework, reservoir computing (RC)[6,42–44]. The Modified National Institute of Standards and Technology (MNIST) database was used as the training task with 12 flexible OECTs forming the reservoir layer and the siganl from the integarated tensile sensor array was used as the test task to further prove the in-sensing computing capibility of the fully-integrated flexible OECT in-sensor computing circuit. As shown in Fig. 5d, the inputdata of RC network was firstly encoded to different binary gate input patterns, where '1' denotes applying a gate voltage (0.4 V) and '0' denotes no voltage is applied (0 V). Then the OECTs-based reservoir layer outputs 16 distinguishable I_{ds} values due to their excellent non-linear transient response (Fig. 5e. A pre-trained single connected layer serves as the output, with performance evaluated by confusion analysis (Fig. S6). The results show $a > 90\%$ accuracy of flexible OECT-based RC (Fig. 5f), permitting their deployment for practical applications such as wearable sensing and computing at the edge.

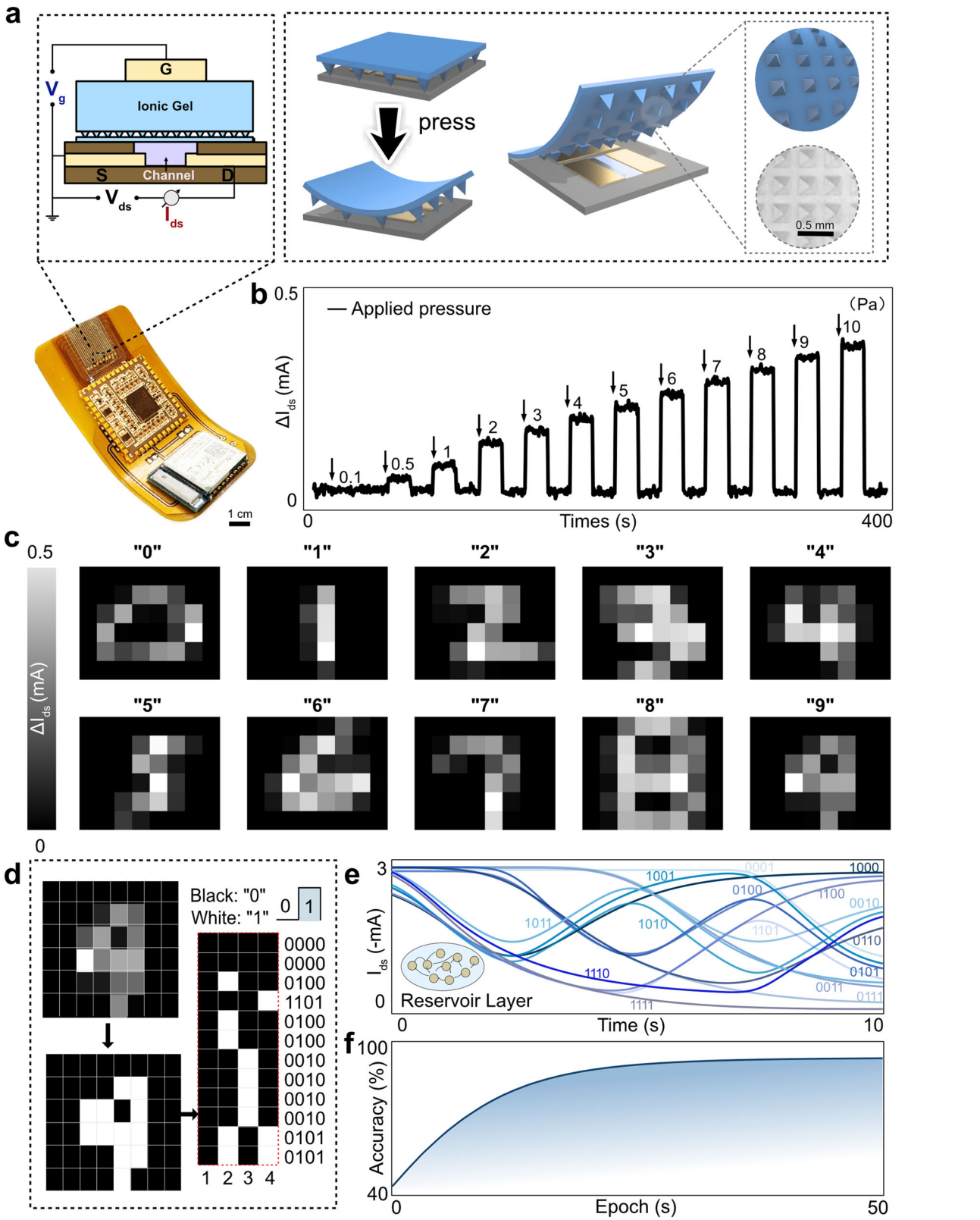

Fig. 5 | Evaluation of flexible OECTs-based in-sensor computing. a shows the schematics of the fPCB-based OECT pressure sensor, also illustrating the sensing mechanism involving a pyramidal ionic gel electrolyte and a real image of the sensor array. **b** shows the variation in sensor current response to discrete pressure gradients. **c** Array of images showing the hand-written characters from "0" to "9" tested using the fPCB-based OECT pressure sensor array. **d** Decoding of the ten digital numbers for RC validation. The grayscale intensity in each image corresponds to the maximum current value detected during a 5-second sensing window. These data serve as a test dataset for reservoir computing applications. **e** The I_{ds} progression curves corresponding to different V_{gs} patterns from 0000 to 1111. **f** Evolution of classification accuracy within 50 training epochs.

In conclusion, we presented a facile and scalable fabrication method that allows large-scale production of flexible all-solid-state OECTs. The electrode arrays and the encapsulation layers were fabricated using mature fPCB technology. The PEDOT:PSS channel and solid-state electrolyte were subsequently patterned on the fPCB with customizable inkjet printing methods. A small feature size of 100 μm was obtained for both the electrodes and the channel. Solid-state gels were found that can avoid the instability of the copper electrodes of the fPCB. Statistical characterizations demonstrated a high device yield (~100%), high homogeneity, and high flexibility were obtained simultaneously. The fast turnaround time, low cost, and scalability of the proposed fabrication methods pave the way for developing flexible solid-sate OECTs (and devices of similar kinds) for practical bioelectronic applications.

Methods

Design and fabrication of fPCB

The circuit diagram of OECT arrays was designed in the lab using open-source electronic design automation software (KiCad). The designed flexible OECT arrays and the fully integrated wearable readout circuit were then manufactured by a commercial fPCB manufacturer (JDBPCB, Shenzhen, China). All electronic components were ordered from DigiKey. The circuit was programmed using the Joint Test Action Group interface, and the circuit firmware was developed in C language (C11/C18). A multilayer fabrication process was used to reduce the size of the PCBs. More details about the readout system can be found in Fig. S7. The battery was connected to a low-dropout linear voltage regulator and the algorithm processing relies on a Bluetooth Low Energy (BLE) system-on-a-chip module (nRF52840, Nordic Semiconductor). For wireless data transmission, the BLE system-on-a-chip uses a miniature ceramic antenna operating at 2.45 GHz.

Preparation of ion gels

Firstly, ionic liquid [BMMIm][TFSI] (97%, Aladdin Co. Ltd., China), monomer EA (99%, Aladdin), crosslinker PEGDA (average M_n 575, Sigma-Aldrich), and photoinitiator 184 (98%, Aladdin) were thoroughly mixed to form a transparent precursor solution. The solution was then patterned onto the devices, bridging the gate electrodes and channel using either drop casting or inkjet printing. Finally, after ultraviolet irradiation (365 nm, 400 W) for 10 min\, the ion gel was fully cured.

Ink-inkjet printing of PEDOT:PSS channel

The PEDOT:PSS suspension was inkjet-printed and patterned between the source and drain electrodes, serving as the channel. Prior to printing, the pristine PEDOT:PSS suspension (Clevios™ PH 1000, Heraeus Electronic Materials GmbH, Germany) was mixed with Capstone FS-30 surfactant (1 v/v%, Sigma-Aldrich), glycerol (5 v/v%, Aladdin), and crosslinker (3-glycidyloxypropyl) trimethoxysilane (GOPS, 1 v/v%, Sigma-Aldrich) to enhance wettability and adhesion to the flexible substrate. The sample was then baked at 80 °C for 20 min, followed by crosslinking at 100 °C for 10 min. Finally, the devices were soaked in deionized water for 2 h to remove the saline from the PEDOT:PSS film. Using our inkjet printing protocol, we were able to achieve a channel thickness of approximately 400 nm, which can also be tuned through adjustments in ink formulation (e.g., dilution level), droplet size, and printing parameters of the inkjet system.

Electrochemical characterizations

The electrochemical characterization was performed with CHI 650E electrochemical workstation (CH Instruments). A standard three electrodes system was built with the fPCB electrode (working electrode), Ag/AgCl electrode (reference electrode), and Pt electrode (counter electrode). The CV measurement was performed in both the ionic gel and phosphate-buffered saline (PBS) solution. The transfer, output, and transient responses of OECTs were measured with Agilent B2902A source-meter unit controlled with Quick IV software.

For the flexibility test, five arched blocks with different radii (from 10 to 50 mm) were fabricated with a 3D printer (Creality CB200) to evaluate the electrical performance of the fPCB-based OECT under different bending conditions.

Data availability

All data supporting the findings of this study are available within the Article and its Supplementary Materials. Additional raw data generated in this study are available from the corresponding authors on reasonable request.

Received: 5 March 2025; Accepted: 10 August 2025;
Published online: 21 August 2025

References

1. Rivnay, J. et al. Organic electrochemical transistors. *Nat. Rev. Mater.* **3**, 17086 (2018).
2. Colucci, R., Barbosa, H. F. D. P., Günther, F., Cavassin, P. & Faria, G. C. Recent advances in modeling organic electrochemical transistors. *Flex. Print. Electron.* **5**, 013001 (2020).
3. Bai, J., Liu, D., Tian, X. & Zhang, S. Tissue-like organic electrochemical transistors. *J. Mater. Chem. C.* **10**, 13303–13311 (2022).
4. Huang, W. et al. Vertical organic electrochemical transistors for complementary circuits. *Nature* **613**, 496–502 (2023).
5. Lee, W. et al. Transparent, conformable, active multielectrode array using organic electrochemical transistors. *Proc. Natl. Acad. Sci. USA* **114**, 10554–10559 (2017).
6. Liu, D. et al. A wearable in-sensor computing platform based on stretchable organic electrochemical transistors. *Nat. Electron.* **7**, 1176–1185 (2024).
7. Zabihipour, M. et al. Organic electrochemical transistors manufactured by laser ablation and screen printing. *Flex. Print. Electron.* **7**, 035018 (2022).
8. Zhang, S. et al. Room-temperature-formed PEDOT:PSS hydrogels enable injectable, soft, and healable organic bioelectronics. *Adv. Mater.* **32**, 1904752 (2020).
9. Kaphle, V., Paudel, P. R., Dahal, D., Radha Krishnan, R. K. & Lüssem, B. Finding the equilibrium of organic electrochemical transistors. *Nat. Commun.* **11**, 2515 (2020).
10. Bernards, D. A. & Malliaras, G. G. Steady-state and transient behavior of organic electrochemical transistors. *Adv. Funct. Mater.* **17**, 3538–3544 (2007).
11. Ghittorelli, M. et al. High-sensitivity ion detection at low voltages with current-driven organic electrochemical transistors. *Nat. Commun.* **9**, 1441 (2018).
12. Kumar, P. et al. Effect of channel thickness, electrolyte ions, and dissolved oxygen on the performance of organic electrochemical transistors. *Appl. Phys. Lett.* **107**, 053303 (2015).
13. Andersson Ersman, P. et al. All-printed large-scale integrated circuits based on organic electrochemical transistors. *Nat. Commun.* **10**, 5053 (2019).
14. Berto, M. et al. Label free urea biosensor based on organic electrochemical transistors. *Flex. Print. Electron.* **3**, 024001 (2018).
15. Guo, K. et al. Rapid single-molecule detection of COVID-19 and MERS antigens via nanobody-functionalized organic electrochemical transistors. *Nat. Biomed. Eng.* **5**, 666–677 (2021).
16. Tian, X. et al. Pushing OECTs toward wearable: development of a miniaturized analytical control unit for wireless device characterization. *Anal. Chem.* **94**, 6156–6162 (2022).
17. Wu, M. et al. Ultrathin, soft, bioresorbable organic electrochemical transistors for transient spatiotemporal mapping of brain activity. *Adv. Sci.* **10**, 2300504 (2023).
18. Khodagholy, D. et al. In vivo recordings of brain activity using organic transistors. *Nat. Commun.* **4**, 1575 (2013).
19. Koutsouras, D. A., Torricelli, F., Gkoupidenis, P. & Blom, P. W. M. Efficient gating of organic electrochemical transistors with in-plane gate electrodes. *Adv. Mater. Technol.* **6**, 2100732 (2021).

20. Harikesh, P. C. et al. Organic electrochemical neurons and synapses with ion mediated spiking. *Nat. Commun.* **13**, 901 (2022).
21. Harikesh, P. C. et al. Ion-tunable antiambipolarity in mixed ion–electron conducting polymers enables biorealistic organic electrochemical neurons. *Nat. Mater.* **22**, 242–248 (2023).
22. Lee, Y. et al. Stretchable organic optoelectronic sensorimotor synapse. *Sci. Adv.* **4**, eaat7387 (2018).
23. Sarkar, T. et al. An organic artificial spiking neuron for in situ neuromorphic sensing and biointerfacing. *Nat. Electron.* **5**, 774–783 (2022).
24. Gkoupidenis, P., Schaefer, N., Garlan, B. & Malliaras, G. G. Neuromorphic Functions in PEDOT:PSS organic electrochemical transistors. *Adv. Mater.* **27**, 7176–7180 (2015).
25. Van De Burgt, Y., Melianas, A., Tom Keene, S., Malliaras, G. & Salleo, A. Organic electronics for neuromorphic computing. *Nat. Electron.* **1**, 386–397 (2018).
26. Andersson Ersman, P. et al. Screen printed digital circuits based on vertical organic electrochemical transistors. *Flex. Print. Electron.* **2**, 045008 (2017).
27. Zabihipour, M. et al. High yield manufacturing of fully screen-printed organic electrochemical transistors. *npj Flexible Elect.* **4**, 15 (2020).
28. Yang, A. et al. Wearable organic electrochemical transistor array for skin-surface electrocardiogram mapping above a human heart. *Adv. Funct. Mater.* **33**, 2215037 (2023).
29. Shim, H. et al. Elastic integrated electronics based on a stretchable n-type elastomer–semiconductor–elastomer stack. *Nat. Electron.* **6**, 349–359 (2023).
30. Chen, S. et al. Ultra-lightweight, highly permeable, and waterproof fibrous organic electrochemical transistors for on-skin bioelectronics. *Adv. Mater. Technol.* **8**, 2200611 (2023).
31. Gao, W. et al. Fully integrated wearable sensor arrays for multiplexed in situ perspiration analysis. *Nature* **529**, 509–514 (2016).
32. Yao, D. R. et al. Anisotropic ion conducting particulate composites for bioelectronics. *Adv. Sci.* **9**, 2104404 (2022).
33. Zhang, S. et al. Water stability and orthogonal patterning of flexible micro-electrochemical transistors on plastic. *J. Mater. Chem. C.* **4**, 1382–1385 (2016).
34. Zhang, Y. et al. Adaptive biosensing and neuromorphic classification based on an ambipolar organic mixed ionic–electronic conductor. *Adv. Mater.* **34**, 2200393 (2022).
35. Liu, D. et al. Intrinsically stretchable organic electrochemical transistors with rigid-device-benchmarkable performance. *Adv. Sci.* **9**, 2203418 (2022).
36. Braendlein, M. et al. Lactate detection in tumor cell cultures using organic transistor circuits. *Adv. Mater.* **29**, 1605744 (2017).
37. Zhang, S. et al. Hydrogel-enabled transfer-printing of conducting polymer films for soft organic bioelectronics. *Adv. Funct. Mater.* **30**, 1906016 (2020).
38. Bai, J. et al. Coin-sized, fully integrated, and minimally invasive continuous glucose monitoring system based on organic electrochemical transistors. *Sci. Adv.* **10**, eadl1856 (2024).
39. Li, Z. et al. Gelatin methacryloyl-based tactile sensors for medical wearables. *Adv. Funct. Mater.* **30**, 2003601 (2020).
40. Ji, X. et al. Mimicking associative learning using an ion-trapping non-volatile synaptic organic electrochemical transistor. *Nat. Commun.* **12**, 2480 (2021).
41. Keene, S. T. et al. A biohybrid synapse with neurotransmitter-mediated plasticity. *Nat. Mater.* **19**, 969–973 (2020).
42. Appeltant, L. et al. Information processing using a single dynamical node as complex system. *Nat. Commun.* **2**, 468 (2011).
43. Pecqueur, S. et al. Neuromorphic time-dependent pattern classification with organic electrochemical transistor arrays. *Adv. Electron. Mater.* **4**, 1800166 (2018).
44. Petrauskas, L. et al. Nonlinear behavior of dendritic polymer networks for reservoir computing. *Adv. Electron. Mater.* **8**, 2100330 (2022).

Acknowledgements

This work was supported by grants from the the Collaborative Research Fund (C7005-23Y) and the Theme-based Research Scheme (T45-701/22-R) from the Research Grants Council of the Hong Kong SAR Government; the Innovation and Technology Fund (Mainland-Hong Kong Joint Funding Scheme, MHP/053/21, MHP/066/20) from the Hong Kong SAR Government; and the Shenzhen-Hong Kong-Macau Technology Research Programme (SGDX20210823103537034) from the Shenzhen Science and Technology Innovation Committee, and the Seed Funding for Strategic Interdisciplinary Research Scheme from the University of Hong Kong (HKU).

Author contributions

S.Z. and X.T. conceived the idea. S.Z. acquired funding for this project and supervised the whole research. X.T., J.B., D.L., and G.L. conducted the experiments and collected the data. X.T. and S. Z., drafted the manuscript. All authors contributed to the revision of the manuscript.

Competing interests

The authors declare no competing interests.

Additional information

Supplementary information The online version contains supplementary material available at https://doi.org/10.1038/s41528-025-00472-x.

Correspondence and requests for materials should be addressed to Shiming Zhang.